Thin Solid Films 519 (2011) 3851–3858

Contents lists available at ScienceDirect

Thin Solid Films

journal homepage: www.elsevier.com/locate/tsf

Transparency and electrical properties of meshed metal films

J. Hautcoeur [a,b], X. Castel [a,*], F. Colombel [a], R. Benzerga [a], M. Himdi [a], G. Legeay [a], E. Motta-Cruz [b]

[a] IETR/UMR CNRS 6164/IUT de Saint-Brieuc, 18 rue H. Wallon, 22004 SAINT-BRIEUC et 263 av. Général Leclerc, Université de Rennes 1, 35042 RENNES Cedex, France
[b] BOUYGUES Telecom, 76 rue des Français Libres, BP 36338, 44263 NANTES Cedex 2, France

ARTICLE INFO

Article history:
Received 19 April 2010
Received in revised form 13 January 2011
Accepted 18 January 2011
Available online 28 January 2011

Keywords:
Optical transparency
Sheet resistance
Gridded metal film
Meshed metal layer
Silver film
Transparent conducting oxide

ABSTRACT

Meshed silver/titanium films, deposited on a 1737 Corning glass substrate by radiofrequency (r.f.) magnetron sputtering and etched by wet process, have been studied. Sputtering parameters have been specifically optimized for thick Ag layer deposition (>3 μm) and are discussed. An original excimer laser etching process is used for removing the resist for making the prototypes. Simple sheet resistance and optical transparency computings have been used for the theoretical study. A good agreement is obtained with the experimental results. Transparent and conducting samples have been realized with optical transmittances and sheet resistances ranging from 71% to 81% and from 0.023 Ω/□ to 1.03 Ω/□, respectively. Hence we demonstrate the independence between optical transparency and sheet resistance for this material AgGL (Ag Grid Layer). The relevance of the mesh structure has been highlighted by the achievement of samples with high level of transparencies and ultra-low sheet resistances.

1. Introduction

Nowadays, many applications need transparent and conductive coatings, like flat panel displays, solar cells, and so on [1]. Up to now, materials belonging to the transparent conducting oxide family (TCO) are routinely used to this end [2]. With a monolayer of TCO material, a resistivity close to 10^{-4} Ω cm is reached with an optical transmittance of about 80% [2]. Guan et al. have elaborated fluorine-doped tin oxide thin films with a 1.9 Ω/□ sheet resistance and 70% of transparency at 550 nm [3]. But this transparency is most often the maximum value achieved in the visible part of the spectrum or an average value lined by extremes of interference fringes (maxima and minima) [4]. Fundamental and experimental researches are very active to improve the conductivity of the materials without damaging their optical transparency. For this purpose, multilayers like TCO–metal–TCO [5,6] or TCO–metal–TCO–metal–TCO [7] have been developed. The embedding of ultrathin metal layer(s) reduces significantly the sheet resistance of samples while preserving their optical properties. For example, a sheet resistance of 1.2 Ω/□ has been reached with a maximum transmittance of 78% at 530 nm [7].

However, this solution implies a limitation of both sheet resistance and optical transparency values. A decrease of the sheet resistance could be easily achieved by increasing the thickness of the embedded metal layer(s), but it will affect strongly the transparency. Note that with a thickness of above 200 nm, a metal thin film becomes totally opaque [8]. With this multilayer technology, it is impossible to reach sheet resistance strongly lower than 1 Ω/□ while preserving the high optical transparency. That is why we propose an original approach to solve the problem of interdependency between sheet resistance and transparency.

In this paper, we are going to report silver/titanium films deposited on glass substrates by radiofrequency (r.f.) sputtering and the fabrication of mesh structures from these bilayers. Sputtering parameters have been optimized in order to synthesize smooth thick Ag films. Two ways have been followed to achieve the mesh structure: an original process is based on a local laser ablation, and another one is based on a conventional standard photolithographic wet etching. A short theoretical study, which is presented in this paper, underlines the independence between the optical transparency and the sheet resistance of such gridded metal layers. At the end, the relevance of mesh structures has been proved by the achievement of samples with high level of transparency and ultra-low sheet resistance.

2. Experimental

2.1. Deposition procedure

Thin films of silver (Ag) and titanium (Ti) are deposited on a 1737 Corning glass substrate by r.f. magnetron sputtering technique at room temperature. The deposition chamber (Plassys MP 450S) is pumped down to 8×10^{-6} Pa by a turbomolecular rotary pump system. This chamber contains two sputtering targets (75 mm diameter): a titanium disc (99.995% purity) and a silver disc (99.99% purity). This configuration makes it possible to grow a monolayer or a multilayer in a complete run without breaking vacuum. A glass substrate

* Corresponding author at: IETR/UMR CNRS 6164/IUT de Saint-Brieuc, 18 rue H. Wallon, 22004 SAINT-BRIEUC et 263 av. Général Leclerc, Université de Rennes 1, 35042 RENNES Cedex, France. Tel.: +33 2 96 60 96 53; fax: +33 2 96 60 96 52.
E-mail address: xavier.castel@univ-rennes1.fr (X. Castel).

0040-6090/$ – see front matter © 2011 Elsevier B.V. All rights reserved.
doi:10.1016/j.tsf.2011.01.262

Table 1
Standard sputtering deposition parameters of Ti and Ag materials.

Layer	Ti	Ag
r.f. power (W)	150	150
Total pressure (Pa)	1.1	1.1
Substrate–target distance (mm)	72	72
Deposition rate (nm min^{-1})	19	146

(50 mm × 50 mm × 0.7 mm) clamped on an oxygen-free high-conductivity copper sample holder is introduced in the deposition chamber via a loadlock chamber. The sample holder revolves around a central axis, which allows positioning substrate in front of the selected target.

During the deposition stage, the working target is supplied with r.f. power through an automatic matching network. The argon gas (99.9996% purity) is bled into the sputtering chamber and is adjusted by a mass flow controller. Sputtering rate has been calibrated for each target. The thickness of each layer is controlled through sputtering time. The deposition parameters are summarized in Table 1. Samples do not undergo any further process in order to improve their properties.

2.2. Fabrication of mesh structures

The first process is used for prototyping different apertures and pitches, taking the advantage of a maskless technology. It uses an excimer laser (Lambda Physics LPX 120 working with KrF — λ = 248 nm) coupled to a work station (optical assembly and *X*–*Y* micrometric moving tables) described in [9]. Tables' movement and laser shots are computer driven. Overall accuracy is 2 μm. A 2.3-μm-thick resist layer (Shipley N49202M), with a high absorption coefficient (α>40000/cm at 248 nm), is spin-coated on Ag. Then, the resist is locally ablated under square laser impacts (frequency 75 Hz, fluence 700 mJ/cm^2, 22 shots/area) in order to print the periodic pattern. Proper heat treatments before and after ablation will take care of smearing and adhesion problems. So, stripped Ag/Ti bilayer can undergo chemical etching through the openings in the resist.

The second process used is a standard photolithographic wet etching. First, the silver film is spin-coated with a photosensitive resist layer (Microposit S1828 Photo Resist from Shipley). Then, the sample is exposed to UV light through a photomask with the appropriate grid pattern. After developing the exposed photoresist, Ag and Ti films are ready to be engraved in suitable chemical solutions. Silver layer is etched in $HNO_3/H_3PO_4/CH_3COOH/H_2O$ solution with a ratio of 1:4:4:1 (v/v) and titanium layer in HF/H_2O solution with a ratio of 3:97 (v/v).

2.3. Characterization methods

A standard 4-point probe configuration, with a 225 Keithley current source and a 7050 Schlumberger microvoltmeter, provides the sheet resistance $R_\square$ at room temperature.

Thin film thickness d is measured with a Tencor Alpha-Step 100 profilometer. Hence, the conductivity σ of the deposited material is deduced from Eq. (1):

$$R_\square = \frac{1}{\sigma d} \tag{1}$$

Optical transmittance is recorded by an UV–Visible spectrophotometer (Perkin Elmer Lambda 20, scanning speed 240 nm/min, 2 nm width slit) in the spectral range of 200–1100 nm, at normal incidence.

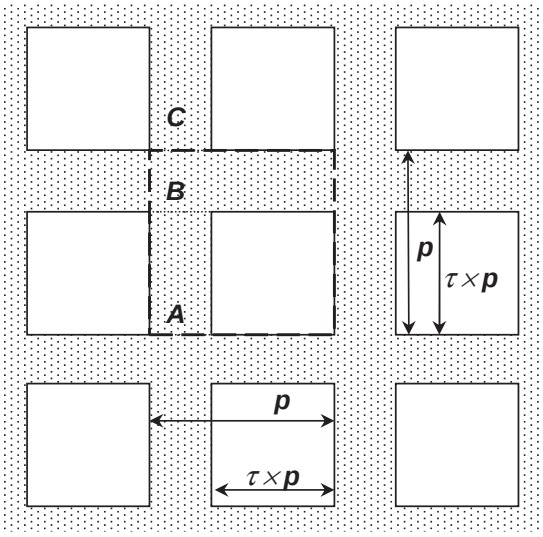

Fig. 1. Schematic representation of a meshed pattern with the relevant square used for $R'_\square$ calculation.

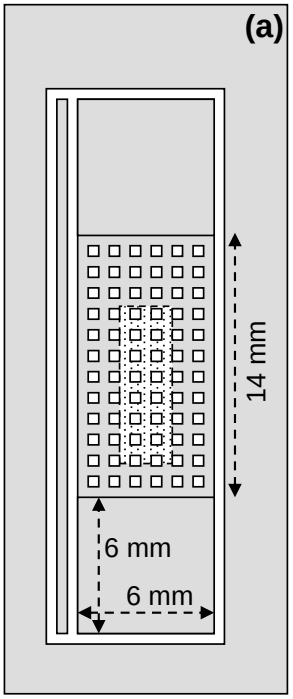

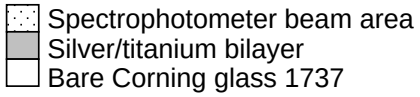

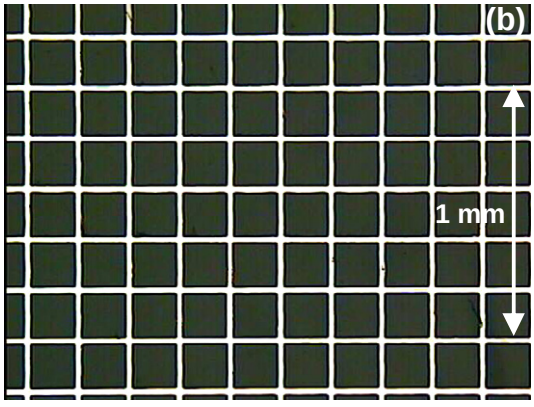

Fig. 2. (a) Layout of the test vehicle. (b) Gridded Ag/Ti bilayer detail with parameters: p = 200 μm, τ = 0.9.

Table 2
Relationship between aperture parameter τ, optical transmission T_r and sheet resistance $R'_{\square}$. Theoretical and experimental values are specified.

Sample	1	2	3	4	5	6
τ parameter	0.85	0.87	0.88	0.90	0.91	0.95
Theoretical T_r (%)	66.5	69.6	71.2	74.5	76.2	83.0
Experimental T_r (%)	67.4	70.0	72.3	75.5	76.1	81.3
Theoretical $R'\square$ (Ω/□)	0.11	0.12	0.13	0.16	0.18	0.32
Experimental $R'\square$ (Ω/□)	0.11	0.13	0.15	0.16	0.18	0.34

The UV–Visible spectrophotometer is already calibrated with air (blank). The values of transmittance of each sample include the Fresnel losses of the glass substrate.

An X-ray diffractometer (Seifert 3003 PTS) in θ–2θ mode is used to determine thin film orientation. A parallel beam configuration is used with a Ge(220) monochromator mounted on the primary beam (Cu $\lambda_{K\alpha 1} = 0.154056$ nm). Data are recorded from 10° to 70° with a step angle of 0.01° and a scan rate of 0.15°/min. Ag indexation is obtained in reference to the joint committee in powder diffraction standards file 04-0783 (Ag crystallizes in face-centered cubic (FCC) structure with a lattice parameter $a = 0.40862$ nm). The degree of mosaicity of silver films in the direction normal to the substrate surface has been checked by ω-scan measurements.

Sample surface morphology is investigated both with a light microscope Leica DMLM and with a Jeol JSM-5600 scanning electron microscope (SEM) operating at 10 kV. The in-depth morphology of films is studied by SEM on cleaved sections.

3. Theoretical assessment of meshed metal film characteristics

3.1. Transparency

The percentage of light transmitted through a meshed metal film is determined by the ratio between aperture area and metal area. The shape of the periodic array is shown in Fig. 1. p is the pitch of the grid, and each square aperture has sides of length $\tau \times p$ with $0 < \tau < 1$. So, the transmission percentage T_{grid} of the configuration is

$$T_{grid} = \frac{(\tau \times p)^2}{p^2} = \tau^2. \quad (2)$$

As meshed metal layers are carried on a substrate, the Fresnel losses due to air/glass interface have to be taken into account. The optical reflectance R is given by [4]

$$R = \frac{\left(n_{glass} - n_{air}\right)^2}{\left(n_{glass} + n_{air}\right)^2}. \quad (3)$$

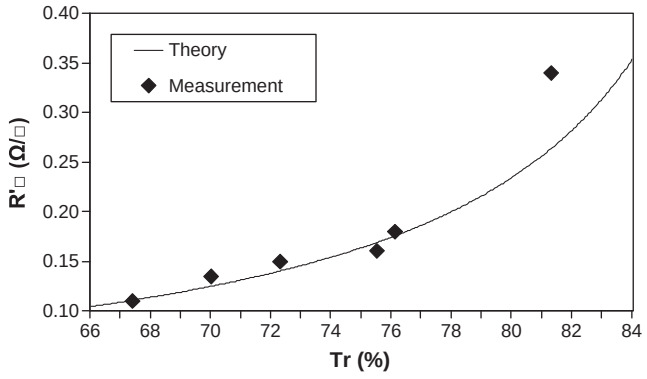

Fig. 3. Sheet resistance $R'_{\square}$ vs. optical transparency T_r. Theory (solid line) and measurement (black diamond). Ag thickness $d = 1$ μm.

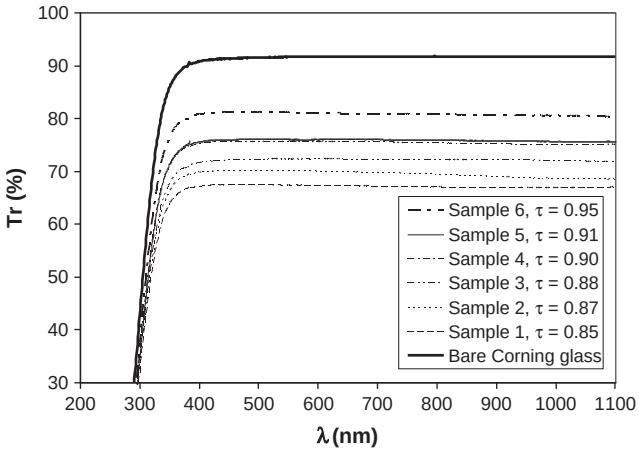

Fig. 4. Transmission spectra of meshed metal films with various τ parameters. For a comparison, the spectrum of bare Corning glass is also plotted.

With an average value of $n_{glass} = 1.52$ for the 1737 Corning glass [10], R is close to 4%. Therefore, the theoretical transparency T_r of meshed samples is given by the formula:

$$T_r = (1-R)^2 T_{grid} = 0.92\,\tau^2. \quad (4)$$

3.2. Sheet resistance

The sheet resistance $R_{\square}$ of a continuous metal film can be safely calculated (Eq. 1) from the bulk metal conductivity, if the film thickness is higher than 1 μm [8].

After mesh structure fabrication, the sheet resistance $R'_{\square}$ increases owing to holes in metal layers. Regarding to electrical behavior, a mesh structure can be described as an array of rectangular metal strips of length $\tau \times p$ and width $p - \tau \times p$, connected together with the help of square nodes of length $p - \tau \times p$ (Fig. 1). As an approximation, the resistance of the node BC is computed at $1 \times R_{\square}$, neglecting a small lateral broadening of the electric field lines out of the square. Thus, for a current propagation along the main direction AC, the resistance $R'_{\square}$ of a square of side length p is equal to $R_{AB} + R_{BC}$ with

$$R'_{\square} = R_{AB} + R_{BC} \approx \frac{\tau \times p}{p - \tau \times p} R_{\square} + R_{\square}. \quad (5)$$

No net current is carried perpendicularly to BC because of equipotential nodes. Then, the sheet resistance $R'_{\square}$ of a square of

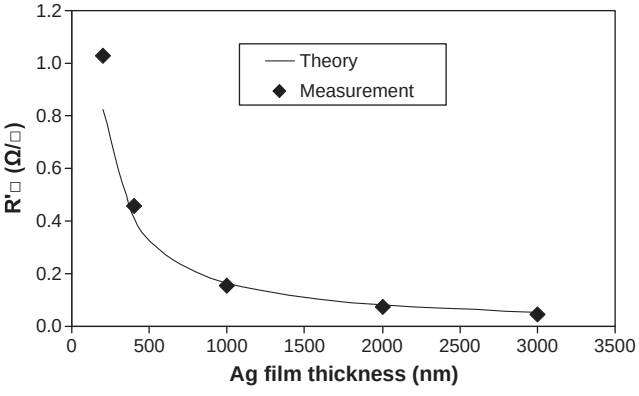

Fig. 5. Evolution of the sheet resistance $R'_{\square}$ vs. Ag film thickness. Theory (solid line) and measurement (black diamond) for an aperture parameter $\tau = 0.9$.

Table 3
Experimental sheet resistance $R'_{\square}$ vs. Ag film thickness, for different aperture parameters τ.

τ parameter	0.90	0.92	0.95
Experimental T_r	≈73%	≈77%	80.6%
Ag thickness			
200 nm	1.03 Ω/□		
400 nm	0.45 Ω/□		
1000 nm	0.16 Ω/□	0.23 Ω/□	
2000 nm	0.07 Ω/□	0.09 Ω/□	
3000 nm	0.05 Ω/□	0.07 Ω/□	0.10 Ω/□

side length p, and so of a meshed metal film, is given by the following relationship:

$$R'_{\square} \approx \frac{1}{1-\tau} R_{\square}. \quad (6)$$

Using Eq. (6) for a meshed metal film with ultra-narrow strips (τ tends to 1), the value of the sheet resistance $R'_{\square}$ tends to infinity. We used computer simulations to estimate the error from the approximation of the BC segment to a perfect square. We broke down a basic pattern ($\tau = 0.9$) into more than 1300 small squares. By applying the Ohm law to each small square and by iterations, $R'_{\square}$ converges to $9.7 \times R_{\square}$ instead of $R'_{\square} = 10R_{\square}$ from (Eq. 6). The same result was obtained for a current flow tilted by 45°.

4. Results

In this work, we have chosen silver (the best metal conductor of the periodic table) for the elaboration of conductive samples ($\sigma_{Ag} = 63.0 \times 10^6$ S/m at 293 K [11]). But, this noble metal shows poor adhesion on an oxide substrate. An ultrathin titanium film (5 nm thick) has been deposited between substrate surface and silver overlayer to

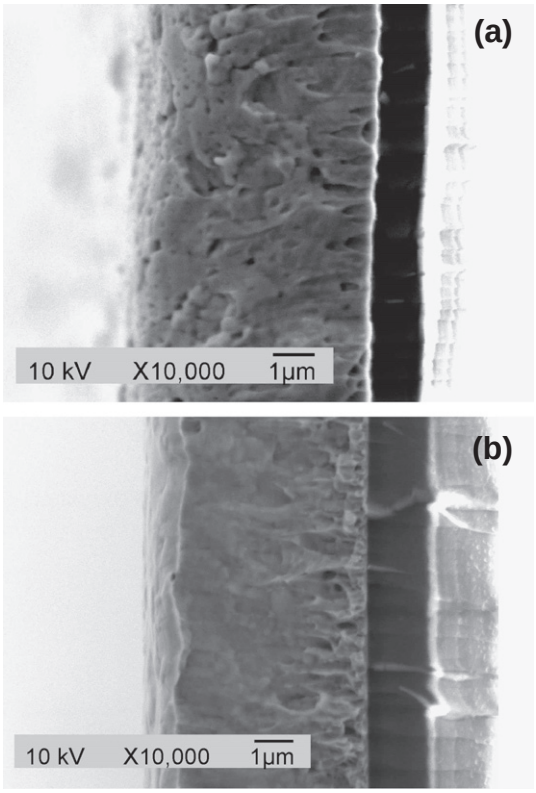

Fig. 7. SEM observations of cleaved 6 μm/5 nm thick Ag/Ti films grown with (a) standard sputtering parameters and (b) thermalized deposition parameters. Scale = 1 μm.

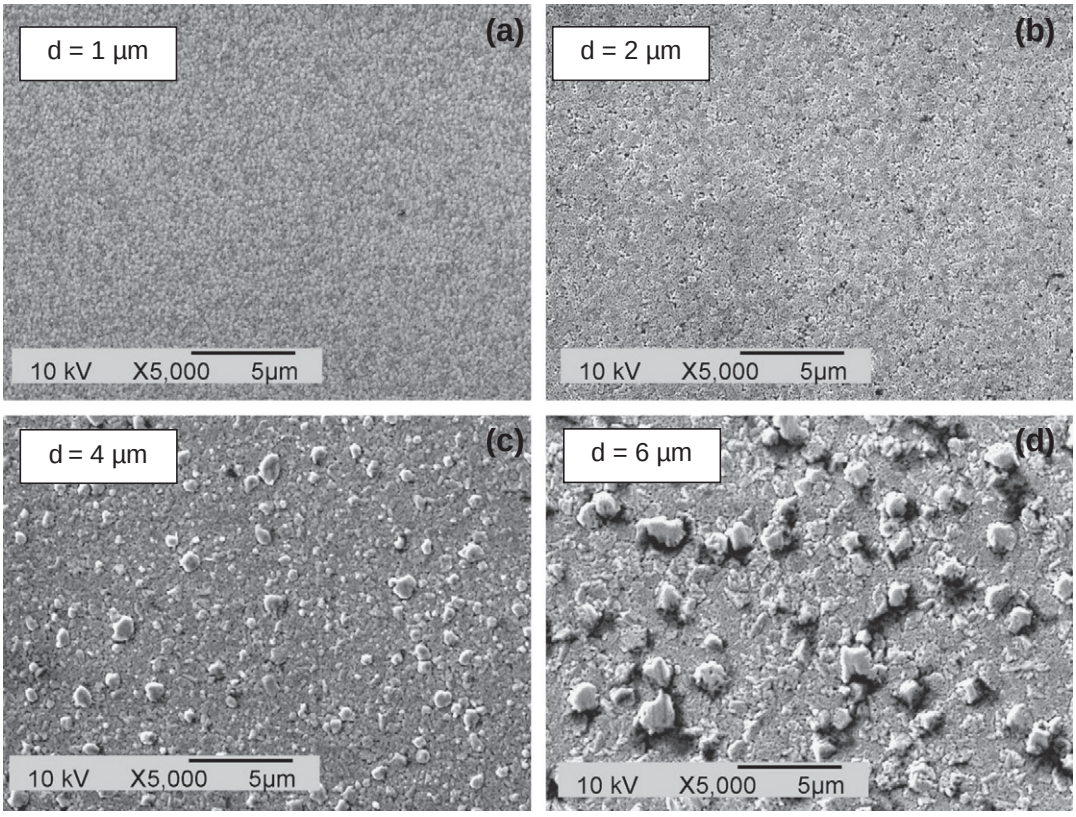

Fig. 6. SEM observations of Ag/Ti films with different Ag thicknesses: (a) 1 μm; (b) 2 μm; (c) 4 μm; (d) 6 μm (standard process). Scale = 5 μm.

ensure strong adhesion. Ag/Ti bilayers are then mechanically stable and are suitable for the preparation of reliable meshed metal films. Due to the low conductivity of titanium ($\sigma_{Ti} = 2.56 \times 10^6$ S/m at 273 K [11]) and its ultrathin thickness, only silver film characteristics affect the sheet resistance values of Ag/Ti bilayers.

4.1. Impact of the aperture parameter τ

In this part, Ag/Ti bilayers with constant film thicknesses (1 μm/5 nm, respectively) are used. τ parameter ranges from 0.85 to 0.95 to achieve theoretical transparency ranges from 66.5% to 83%. Meshed samples have been built by the excimer laser ablation process.

The test vehicle is shown in Fig. 2. On the left side, a continuous metal strip of 26 squares is kept with no hole in order to check the basic value of $R_{\square}$. All test samples provide $R_{\square}$ equal to 0.016 Ω/□, which is consistent with theoretical value given by Eq. (1). The gridded area, delimited by two continuous squares, is large enough to include the analysis window of spectrophotometer and relevant for four-wire resistance measurements. The knowledge of both square number in the gridded area and $R_{\square}$ value enable us to extract experimental $R'_{\square}$ sheet resistance.

The aperture parameter influence on optical transparency and sheet resistance is summarized in Table 2. Experimental values range from 67.4% to 81.3% and from 0.11 Ω/□ to 0.34 Ω/□, respectively. Measurements (Fig. 3) fit closely with the curve, resulting from Eqs. (4) and (6):

$$R'_{\square} = \frac{0.96}{0.96 - \sqrt{T_r}} R_{\square}. \quad (7)$$

The approximation error from (Eq. 6) is hidden by the experimental errors.

With great interest, each test sample shows a plateau on transmission curve for wavelength upper than 400 nm (Fig. 4). Under 400 nm, transmittance falls down due to Corning glass absorption (band gap). So in the visible part of the spectrum, the optical transparency T_r of meshed metal films is strictly constant. Its level is adjusted by τ value, independently from the pitch of grid p. We have checked that test samples with p parameter equal to 100 μm, 200 μm, 300 μm and 400 μm supply similar data.

These results show that transparency level of the structure is adjustable. But it impacts directly the sheet resistance value (Eq. 7), when the Ag layer thickness is kept constant.

4.2. Impact of Ag film thickness

To study the effect of Ag film thickness on the electrical behavior of the mesh structure, we have worked with a constant mesh strip-spacing ($\tau = 0.9$ which fixes a theoretical transparency $T_r = 74.5\%$). In this case, the photolithographic process is relevant because we use only one photomask (it is laid out by taking into account over etching); it is a suitable process for industrial applications and process time is not commensurate to sample area (unlike with the laser ablation process).

Five gridded metal layers, with a thickness ranged from 200 nm to 3 μm, have been built on 50 mm × 50 mm Corning glass. The measured evolution of $R'_{\square}$ versus Ag film thickness is shown in Fig. 5. Theory (Eq. 6) and measurement match very well. Measured optical transmission ranges from 71% to 74.5% (it depends on over-

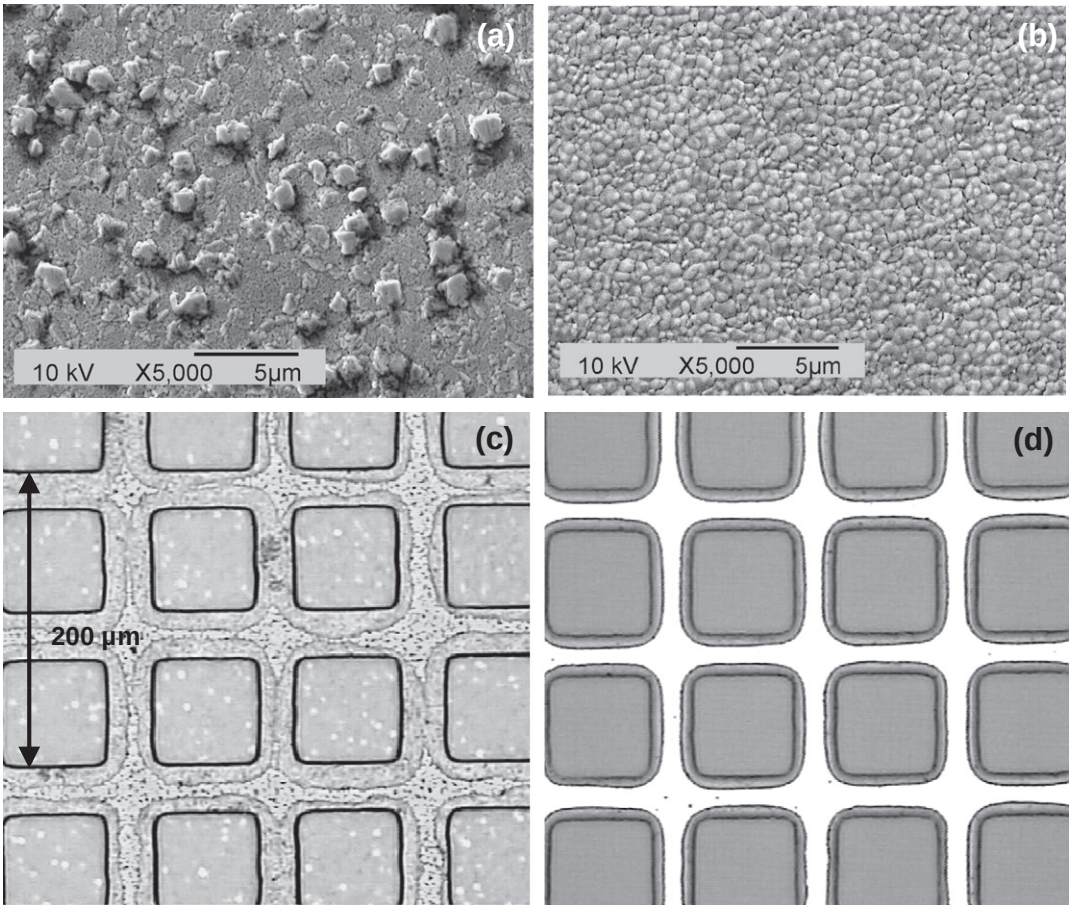

Fig. 8. SEM observations of 6 μm/5 nm thick Ag/Ti films grown with (a) standard sputtering parameters and (b) thermalized deposition parameters. Optical microscopy observations after wet etching and without photoresist stripping of 6 μm/5 nm thick Ag/Ti films grown with (c) standard sputtering parameters and (d) thermalized deposition parameters.

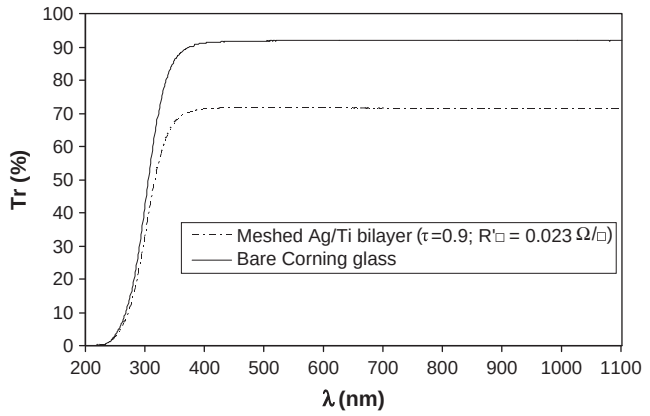

Fig. 9. Transmission spectra of a 6 μm/5 nm meshed Ag/Ti bilayer. For a comparison, the spectrum of bare Corning glass is also plotted.

etching adjustment), which is agreeable with our needs. Our highest sheet resistance, close to 1 Ω/□, reaches the best result of the state of art achieved with TCO–metal–TCO–… multilayer reported in [7].

Other samples have been built with different Ag film thicknesses and three different levels of transparency (see Table 3). It shows that an identical sheet resistance can be obtained with different optical transmittances, with the help of an aperture adjustment and by adjusting the Ag film thickness.

4.3. Mesh structure technological restrictions and deposition step improvement

To further demonstrate the interest of meshed metal film solution, we finally designed a high-transparency sample having a sheet resistance close to that of a continuous 1-μm-thick silver film (0.016 Ω/□).

Theoretically, a 6-μm-thick silver layer gridded with $\tau = 0.9$ will ensure an optical transmission and a sheet resistance equal to 74.5% and 0.026 Ω/□, respectively. However, with the growth parameters given in Table 1, sputtering emphasizes the roughness of thick silver films (above 3 μm, Fig. 6). For a 6 μm, an average grain size ranges between 1 μm and 2 μm. Furthermore, voids are suspected in the depth of the layer (Fig. 7a). With such an Ag morphology, over-etching cannot be controlled any more, inducing the consumption and vanishing of many strips (Fig. 8c).

To restore the microstructure of lower thickness Ag samples, sputtering parameters have been changed. We have increased the r.f. power (300 W) and cut the silver run deposition in two successive steps: 600 nm Ag growth forwarded by 5 min cooling time, keeping on the argon gas flow. These two steps are repeated up to reach the total Ag thickness. With these parameters, thick Ag layers have been grown with even microstructure (Fig. 7b) and surface (Fig. 8b). So over-etching can be perfectly controlled (Fig. 8d). A 6-μm-thick meshed layer is finally obtained. Its optical transmission reaches the expected values of 71.1% (Fig. 9) with $R'_{\square} = 0.023$ Ω/□.

5. X-ray diffraction and discussion on the metal texture

Silver films show (111) out-of-plane texture [12]. This is consistent from a thermodynamic point of view. Metal thin films crystallize with preferred orientations along directions perpendicular to the planes of lowest surface energy [13]. Metal FCC structures, like silver, correspond to the most densely packed planes, i.e., (111) planes [14].

Thick Ag layer (6 μm) grown with standard sputtering parameters (Table 1) shows pure (111) orientation (Fig. 10a). Lattice constant *a*, calculated from position of the (111) diffraction peak matches perfectly theoretical value (0.408 nm), indicating Ag layer without strain. Rocking-curve around the diffraction peak exhibits $\Delta\omega$ value of 2.0°. An average silver particle size ε was calculated from Scherrer formula, $\varepsilon = \frac{\lambda}{\Delta(2\theta)\cos\theta_0}$, where λ is the X-ray wavelength, θ_0 is the Bragg angle; $\Delta(2\theta) = \Delta(2\theta)_{meas} - \Delta(2\theta)_{ap}$ with $\Delta(2\theta)_{meas}$ is the full width at half maximum of $2\theta_0$ peak measured on X-ray diffraction (XRD) pattern and $\Delta(2\theta)_{ap}$ is the apparatus function (in our case, the full width at half maximum of (111) 2θ peak measured on perfect silicon single crystal ($\Delta(2\theta)_{ap} = 0.011°$). A value of 41 nm is obtained. Reflection from the underlying Ti layer has not been observed.

During the deposition step, the diffusivity D_s of metal adatom on metal surface is explained in [15]: $D_s = D_0 \exp\left(-\frac{E_D}{kT}\right)$, where D_0 is a prefactor and E_D is the activation energy for surface diffusion. Silver adatom mobility would be proportional to D_s. The growth of thick Ag layer leads to long deposition time (41 min) and an increase of the substrate surface temperature. It induces better adatoms mobility and

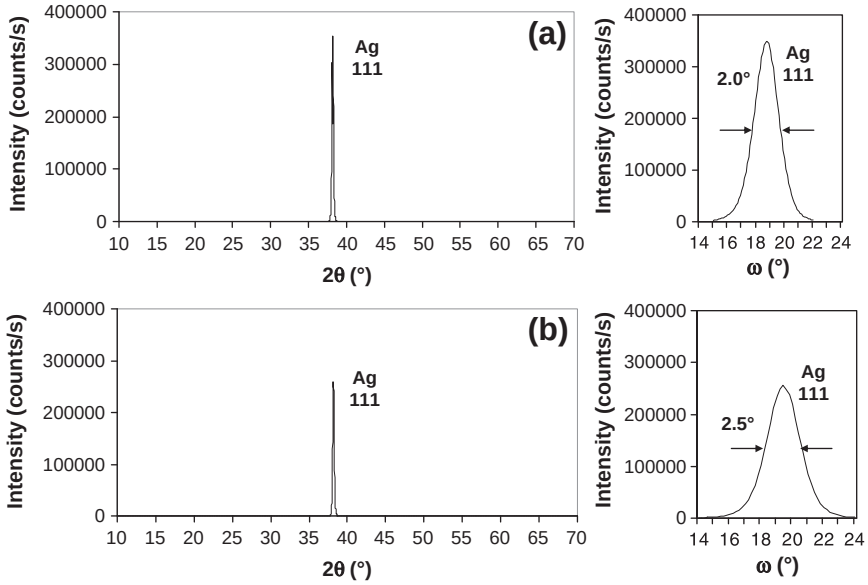

Fig. 10. XRD patterns in θ–2θ mode and ω-scan around (111) Ag peak on 6 μm/5 nm thick Ag/Ti bilayers grown with (a) standard sputtering parameters and (b) thermalized deposition parameters.

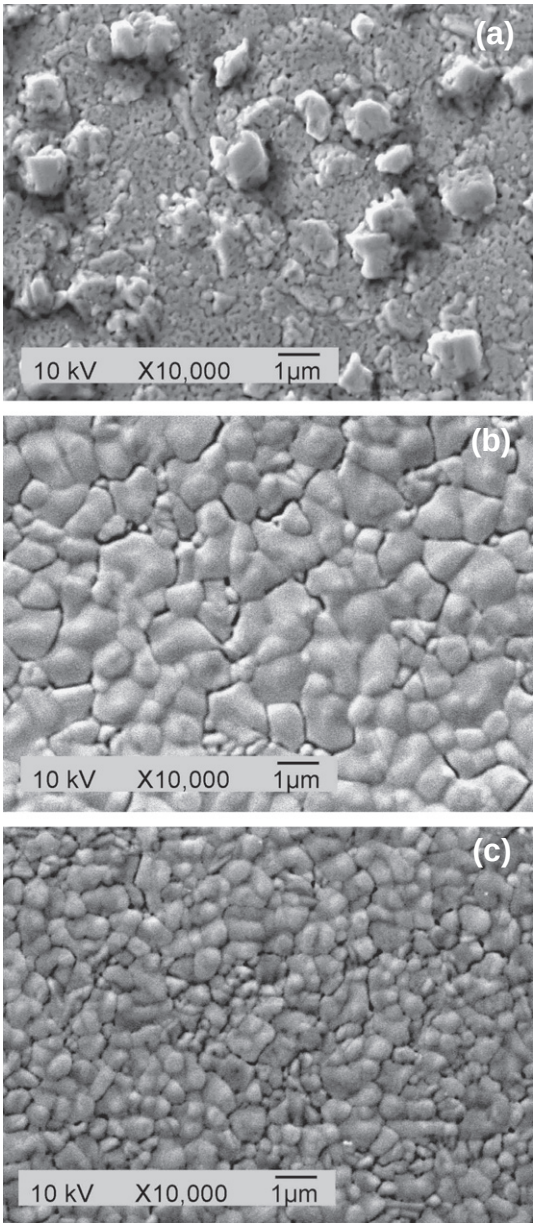

Fig. 11. SEM observations of (a) 6 μm/5 nm thick Ag/Ti films grown with standard sputtering parameters, (b) 150 W sputtering power with thermalization steps, and (c) 300 W sputtering power with thermalization steps.

gives to the adatoms a possibility to reach easily grains with lower surface energy. Then, thick Ag layer grows with strong columnar structure along (111) direction. The silver grains observed on SEM pictures (Fig. 6) would be the tips of columns. Note that columns and tips are built of agglomerated silver particles, each one of individual size ε.

We assumed that limiting the adatom mobility on the surface would restrict the silver columnar growth. According to Jung [16], the average distance that an adatom can move in a time t is $\sqrt{2D_s t}$. An increase of the deposition rate would reduce the delay t until an adatom is covered by new Ag atoms. Thus, the distance at which adatom could find a grain with a low surface energy is reduced. Consequently, sputtering power was doubled (300 W) in order to quickly bury silver adatoms by the incident atom flux. But higher r.f. power means increased surface temperature and so, higher D_s. That is why a 5-min cooling time has been used between two successive deposition steps. The 6-μm-thick Ag layer sputtered with these thermalized deposition parameters keeps (111) orientation (Fig. 10b). The intensity of XRD peak decreases (from 353 kcounts/s to 258 kcounts/s) and the rocking-curve gets wider ($\Delta\omega = 2.5°$). That means lower crystallinity, a restriction of columnar growth of the sample and a higher film density. These results are confirmed by SEM observations (Figs. 7 and 8). The lattice constant a and the average silver particle size ε are retained (0.408 nm and 43 nm, respectively).

Note that the deposition at 150 W, using only the cooling steps, brings a limited improvement. Hillock formation is suppressed (Fig. 11a and b). But, the average grain size on SEM picture is kept larger than 1 μm. Intensity of the (111) Ag peak (343 kcounts/s) and its rocking-curve ($\Delta\omega = 1.9°$) are similar to those of an Ag/Ti film grown with standard sputtering parameters (Fig. 10a). Therefore, the increase of sputtering power from 150 W to 300 W with thermalization steps limits silver adatom mobility and thus the average grain size (Fig. 11c).

We would highlight that thermalized growth is not relevant for Ag layer when the thickness is thinner than 3 μm. Thermal inertia of the copper sample holder seems sufficient to moderate the increase of the substrate temperature.

6. Conclusion

In this work, we have elaborated transparent and conducting films based on meshed metal layers. High optical transparencies and ultra-low sheet resistances have been obtained. The values for the best sample are $T_r = 71.1\%$ and $R'_{\square} = 0.023\ \Omega/\square$, respectively, which are the lowest paired values reported. Independency between the optical transparency and the sheet resistance was also demonstrated.

According to our work, the design of meshed metal films involves (i) the selection of the grid pitch in accordance with visual acuity and available technology; (ii) the specification of the optical transparency of samples, which gives the value of the parameter τ; (iii) and the specification of the sheet resistance, which gives the required thickness of metallization. Note that a given optical transparency ($\approx 74\%$) can be achieved on a large scale of sheet resistance values from 1.03 Ω/□ to 0.023 Ω/□, in this work. Low limits on the pitch of gridded metal layers come only from technological issues. In this paper, two microtechnologies have been used to build the array of metal strips. Submicronic technology could achieve strip structures of about a few hundred of nanometers [17]. At the opposite way, visual acuity limits the upper level of meshed metal film solution. At near-point viewing distance (0.25 m), the normal visual acuity of the human eye is close to 100 μm [18]. So, a square periodic array with a pitch of 100 μm and metal strips of 10 μm deposited on glass substrate appears to most people as a transparent sample.

Meshed metal films can stand for classical TCO films in case of flat panel display applications. The low sheet resistances will reduce ohmic losses of long feed lines. For solar cell applications, the contact lines made of opaque metal will be judiciously replaced by meshed metal stripes to increase transparency without worsening ohmic losses. A direct application of the meshed metal films is described in [19]. A transparent monopole antenna made from such a material provides high radioelectrical performances, close to those of an opaque antenna made of a continuous metal layer. Such results cannot be achieved by using a standard transparent and conducting material like TCO monolayer or TCO–metal–TCO multilayer, due to detrimental ohmic losses [8].

References

[1] G.J. Exarhos, X.D. Zhou, Thin Solid Films 515 (2007) 7025.
[2] T. Minami, MRS Bull. 25 (2000) 38.
[3] N. Guan, H. Furuya, K. Himeno, K. Goto, K. Ito, the International Workshop on Antenna Technology Proceedings, Cambridge, UK, 2007, p. 263.
[4] R. Swanepoel, J. Phys. E Sci. Instrum. 16 (1983) 1214.
[5] A. Klöppel, W. Kriegseis, B.K. Meyer, A. Scharmann, C. Daube, J. Stollenwerk, J. Trube, Thin Solid Films 365 (2000) 139.
[6] D.R. Sahu, S.Y. Lin, J.L. Huang, Thin Solid Films 516 (2008) 4728.
[7] A. Klöppel, B. Meyer, J. Trube, Thin Solid Films 392 (2001) 311.

[8] F. Colombel, X. Castel, M. Himdi, G. Legeay, S. Vigneron, E. Motta Cruz, IET Sci. Meas. Technol. 3 (2009) 229.
[9] G. Legeay, X. Castel, R. Benzerga, J. Pinel, Phys. Stat. Sol. C 5 (2008) 3248.
[10] Corning 1737 AMLCD Glass Substrates – Material information, MIE101 (2002).
[11] D.R. Lide, Handbook of Chemistry & Physics, 82nd Ed.CRC Press LLC, 2001–2002.
[12] S. Szunerits, X. Castel, R. Boukherroub, J. Phys. Chem. C 112 (2008) 10883.
[13] X. Sun, R. Hong, H. Hou, Z. Fan, J. Shao, Thin Solid Films 515 (2007) 6962.
[14] Y. Tian, H. Liu, G. Zhao, T. Tatsuma, J. Phys. Chem. B 110 (2006) 23478.
[15] G. Antczak, G. Ehrlich, Surf. Sci. Rep. 62 (2007) 39.
[16] Y.S. Jung, Appl. Surf. Sci. 221 (2004) 281.
[17] F. Cui, W. Chen, W. Zhang, Q. Xiao, G. Ma, W. Liu, Microsyst. Technol. 15 (2009) 1885.
[18] D. Cline, H.W. Hofstetter, J.R. Griffin, Dictionary of Visual Science, 4th Ed. Butterworth-Heinemann, Boston, 1997.
[19] J. Hautcoeur, F. Colombel, X. Castel, M. Himdi, E. Motta Cruz, Electron. Lett 45 (2009) 1014.